







ASSESSING SPATIAL AND TEMPORAL PRECIPITATION DYNAMICS IN UPPER EAST REGION OF GHANA USING CHIRPS DATA FROM 1981 TO 2016

 **Thomas Moore Okrah**^{1*}

 **J. A. Quayeballard**²

 **S. A. Andam-Akorful**³

 **Ibrahim Abdul Sulemana**⁴

^{1,2,3}Department of Geomatic Engineering, Kwame Nkrumah University of Science and Technology (KNUST), Kumasi, Ghana.

¹Email: otom789@gmail.com Tel: 0233245264730

²Email: quayeballard@yahoo.com Tel: 086183551007414

³Email: aaakorful@gmail.com Tel: 0233209104956

⁴Pan African University Institute of Earth and Life Science Including Agriculture (PAULESI), University of Ibadan, Nigeria.

⁴Email: Kalibradus26@gmail.com Tel: 0233544996813



(+ Corresponding author)

ABSTRACT

Article History

Received: 13 August 2019

Revised: 17 September 2019

Accepted: 21 October 2019

Published: 9 December 2019

Keywords

Cumulative residual analysis (CRA)

Mann-Kendall and Sen's Slope tests

Wavelet transform (WT)

Principal component analysis (PCA)

Remote sensing

Ghana

CHIRPS data.

Precipitation variability evaluation assumes a vital part in water asset administration and rainfed agribusiness. In Ghana, rain gauge stations are poorly distributed and also, obtaining long time span of data is difficult due to data inconsistency, as a result remotely sensed precipitation products are largely used to complement ground gauge stations data for assessing climatic variability and water resource managements. In this study, Climate Hazards Group Infrared Precipitation with Station (CHIRPS) precipitation data from 1981-2016 and also utilizing Cumulative Residual Analysis (CRA), Mann-Kendall, Sen's Slope, Wavelet Transform (WT) and Principal Component Analysis (PCA). Results show that 1981, 1999, 2002 and 2013 were four noteworthy years with changes in precipitation. The Mann-Kendal and Sen's Slope demonstrate that 55.71% of UER indicated diminishing month to month precipitation with 27.34% critical patterns. Precipitation in April, May, and June demonstrated a diminishing pattern while July, August, and September showed an increasing trend during the 35 years' study period. Further investigation using Continuous Wavelet Transform indicated an annual variation significant. PCA uncovered that the spatial variability of precipitation in UER is extremely assorted, however greater part (33.76%) of the fluctuation is situated in the north-eastern part. Thus, the results from remotely sensed precipitation products an effective, efficient and cheap way of assessing top to the bottom comprehension of precipitation variation at regional level.

Contribution/Originality: This study is one of very few studies which have investigated in the study area which applied new methods such as Cumulative residual analysis (CRA), Mann-Kendall and Sen's Slope tests, Wavelet transform (WT), Principal component analysis (PCA) on remotely sensed precipitation data to assess both spatial and temporal variability.

1. INTRODUCTION

Climatic variability is a key factor influencing African economy and it demonstrates high spatial and temporal varieties at various time scale (Mbereggo *et al.*, 2013). Despite the fact that atmosphere factors, such as, temperature, soil moisture, relative humidity and wind indicated variation on both spatial and temporal scale. Precipitation displays high variability in both space and time (Kabo-bah *et al.*, 2016; Andam-Akorful *et al.*, 2017; Awotwi *et al.*,

2017; Quagraine *et al.*, 2017). Regardless of the high precipitation variation, Ghana depends highly on rainfed agriculture, thus make Ghana valuable to climatic variability due to limited resources (Antwi-Agyei *et al.*, 2012). Precipitation in Ghana has demonstrated intra-seasonal, inter-seasonal and decadal variation throughout the years (Baidu *et al.*, 2017). This influences agribusiness since it utilizes around 70% of the aggregate populace, contributing around 28% to the country Gross Domestic Product (GDP) (Baidu *et al.*, 2017; Quagraine *et al.*, 2017).

In the northern part of Ghana, late precipitation variation has brought about decrease in yield of crop products, migration and relocation as a method of adapting to periodic precipitation changes (Yiran *et al.*, 2012; Jarawura, 2013). Furthermore, dry spell occurrence in the 1980s, 1990s and 2000s have brought about low level in water bodies. Also, high demand for cheap hydro-electrical energy notwithstanding increase in population has resulted in competition for water in the Volta basin (Leemhuis *et al.*, 2009). With a specific end goal to alleviate the impact of precipitation variability in northern Ghana, various small water dams for cultivating and residential utilization have been developed (Nick *et al.*, 2001). Accordingly, understanding spatial and temporal variation in precipitation will give a knowledge into the management and arranging of precipitation subordinate exercises e.g. cultivating, dam administration, and so forth (Basalirwa *et al.*, 1999; Kolivras and Comrie, 2007; Nischitha *et al.*, 2014).

Different investigations on precipitation dynamics in West Africa detailed a diminishing pattern in the 1970's and 1980's and an increasing pattern in precipitation amid 1990's which they depict as dry spell recuperating period (Lacombe *et al.*, 2012; Kabo-bah *et al.*, 2016; Baidu *et al.*, 2017; Quagraine *et al.*, 2017). For instance, Andam-Akorful *et al.* (2017) examine on sustainable water accessibility and they demonstrated precipitation in west Africa indicated interdecadal fluctuation, with the most recent 10 years (from the 2000s) demonstrating a diminishing precipitation drift. Notwithstanding, a report from the Inter-Governmental Panel on Climate Change (IPCC) uncovered that losses in rain-encouraged farming is probably going to increment because of incessant events of the dry season and flooding occasions because of the heightening of the hydrologic cycle (IPCC, 2007). There is, subsequently, the need to evaluate the spatial and transient measurements of precipitation variability in the UER. There is likewise the need to decide the progressions happening in precipitation time arrangement. This will advance economical administration choices.

Ghana has seen exceptional little study in employing remotely sensed precipitation data in assessing fluctuations in precipitation at regional scale. In order to model or monitor drought and flood spells, a predictable and dependable precipitation data as the primary info parameter is required (Wang *et al.*, 2016). In this research, the gridded precipitation data from the Climate Hazards Group Infrared Precipitation with Station (CHIRPS) was utilized to supplement gauge stations information because of the absence of dense rain measure stations, hence CHIRPS precipitation dataset was utilized to study precipitation variations in the Upper East region of Ghana. The decision for choosing this precipitation data is because of its long-time span from 1981 to present, has a generally high spatial resolution (0.05°) and its better validation performance in some part of the world (Le and Pricope, 2017; Paredes-Trejo *et al.*, 2017; Retalis *et al.*, 2017). The long-time span of the CHIRPS precipitation data is valuable to long-haul study of precipitation fluctuation, giving top to the bottom comprehension of precipitation variability and the subsequent effects on rain-fed agriculture in UER. Consequently, the goal of the present study is therefore to study the spatial and temporal dynamics of precipitation in UER. In this manner, the Mann-Kendal test and Sen's Slope estimator were utilized to determine trends patterns; while the Cumulative Residual Analysis (CRA) was utilized to recognize changes in precipitation time series. Also, precipitation periodicity in UER was examined with Wavelet Transforms (WT) and Principal Component Analysis (PCA) to evaluate the spatial and temporal dynamics of precipitation.

2. MATERIALS AND METHODS

2.1. Study Area

UER is situated in the North-Eastern part of Ghana [Figure 1](#). It lies between latitude $10^{\circ} 20' N$ and $11^{\circ} 12' N$ and longitude $0^{\circ} 03' E$ and $1^{\circ} 25' W$. It has an aggregate land surface of around 8,842 square kilometers, covering 2.7% of the aggregate land front of Ghana ([Ghana Statistical Service, 2010](#)). The region shares boundary toward the north with Burkina Faso, toward the east with Togo, toward the west with Upper West Region and toward the south with North-East Region. The atmosphere of the UER is dry sub-sticky and normal day by day temperatures is around $38^{\circ}C$. The locale encounters a unimodal precipitation design which begins in April/May and tops in August before it ends in October. The geography is a delicate slant and the vegetation is Sudan Savannah with short grasses and wide scattered Shrub ([Yiran et al., 2012](#)). The region is drained by the Red, White Volta river and additionally the Sissili River with little dam supplies for irrigation system used in cultivating and residential use amid the dry season ([Leemhuis et al., 2009](#)). The area is described by climatic varieties because of low precipitation occurrences, high temperatures, deforestation and overgrazing ([Ministry of Food & Agriculture, 2017](#)). The principal monetary activities of the general population are farming utilizing around 80% of the aggregate populace, while the rest engaged in trading and craftsmanship like cloth weaving and basketry ([GSS, 2010](#)).

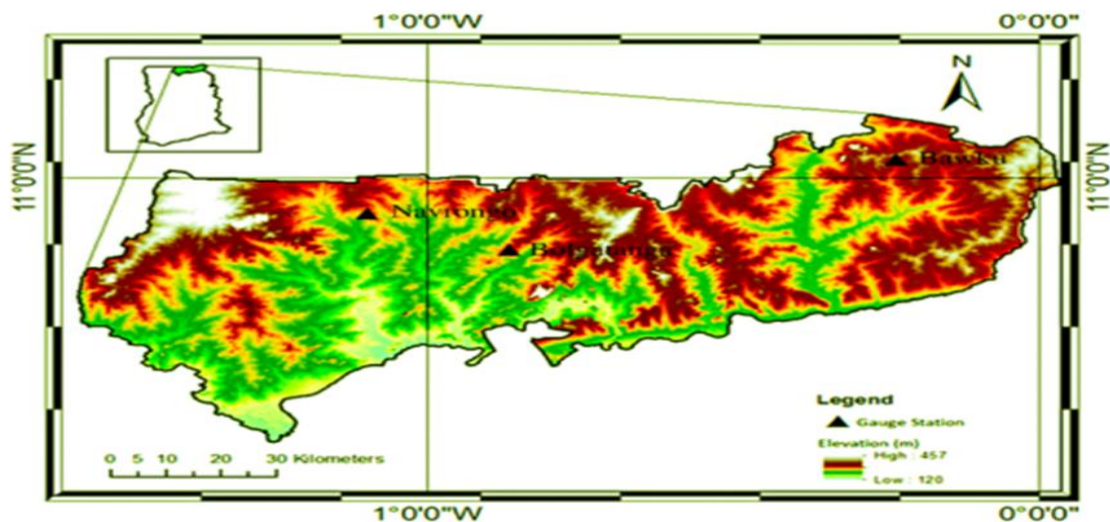


Figure-1. Location of upper East region and rain gauge stations, Ghana.

Source: 30-meter SRTM Digital elevation model from mapping the earth- the shuttle radar topography mission.

2.2. Data Description

CHIRPS data is a freshly precipitation estimate product with the principal mission of checking worldwide dry spell occurrences. What makes CHIRPS data one of a kind from the rest is its high spatial resolution and long-time span ([Le and Pricope, 2017](#); [Retalis et al., 2017](#)). It embraces worldwide infrared data from TRMM geostationary satellite, atmospheric precipitation model forecast system framework from National Oceanic and Atmospheric Administration and consolidate check gauge station information from a various part of the globe to make a high spatial resolution of 0.05° and a temporal resolution at near real-time and monthly time scale. Since its interception, different studies have been led to evaluate it precision and connected in different hydrological models. For instance, [Le and Pricope \(2017\)](#) utilized it to evaluate the exactness of Runoff and Streamflow in Kenya, while [Paredes-Trejo et al. \(2017\)](#) approved it over Northern Brazil and [Retalis et al. \(2017\)](#) resampled it to a $1km \times 1km$ resolution and assessed it with gauge station data in Cyprus. In every one of these studies, CHIRPS precipitation data showed extraordinary performance and results. The CHIRPS precipitation data was freely download and assessed. (<ftp://chg-ftpout.geog.ucsb.edu/pub/org/chg/products/CHIRPS-2.0/>).

2.3. Methods

The methods used to analysed precipitation time series are: (1) Mann-Kendall Test and Sen's Slope to recognize trends in precipitation time series at 95% certainty interim; (2) Cumulative Residual analysis to identify changes in precipitation; (3) Wavelet Transform to comprehend the periodicity in precipitation time series; and (4) Principal Component Analysis (PCA) to determine the spatial and temporal dynamics in precipitation across the study territory. In this investigation, the Morlet mother wavelet was used because of its capacity to provide balance between time and frequency localization, incorporate a wave of certain period, determine time-dependent amplitude and frequency shift phase (Dyn *et al.*, 2016). This is appropriate in examining varieties in atmosphere time arrangement (e.g. (Torrence and Compo, 1998; Liang *et al.*, 2011; Santos and Freire, 2012; Dyn *et al.*, 2016)).

2.3.1. Mann-Kendall (MK) Trend Test

MK is a statistical technique for testing pattern in time series (Blain, 2013). It is a non-parametric and accordingly, does not make any assumption in the time series. This makes it an effective tool for recognizing patterns in climatic factors which are non-stationary and has been suggested by the World Meteorological Organization (WMO) (Liang *et al.*, 2011; Nalley *et al.*, 2013). MK tests for the null hypothesis (H0) of pattern truant against an alternative hypothesis (H1) of pattern exhibit in a time series at a given certainty level. The implementation of MK is depicted in (see (Liang *et al.*, 2011; Blain, 2013; Nalley *et al.*, 2013)). For a given time series (x) with length (N), the test measurement (a method for looking at Ho and H1) is given by Equation 1 (Blain, 2013; Dawood and Atta-ur-Rahman, 2017):

$$\text{Test statistic (t)} = \sum_{i=1}^{N-1} \sum_{j=i+1}^N \text{sgn}(x_j - x_i) \text{ where } j > i \tag{1}$$

If $N > 8$ then the time series is assumed to be normal distributed with a zero mean (Baidu *et al.*, 2017) and variance (V) is computed from Equation 2;

$$V = N(N-1)(2N+5) - \sum_{y=1}^{GG} ti(y-1)(2y+2)y / 18 \tag{2}$$

Where GG = number of groups and ti = length of GG^{th} group

The test statistic(t) is standardized and the significance is also estimated by Equation 3.

$$z = \left\{ \begin{array}{l} \frac{t-1}{\sqrt{V}} \rightarrow t > 0 \\ 0 \rightarrow t = 0 \\ \frac{t+1}{\sqrt{V}} \rightarrow t < 0 \end{array} \right\} \tag{3}$$

The null hypothesis is accepted if $|Z| \leq Z_{1-\alpha/2}$, otherwise H_1 is accepted at α significant level.

2.3.2. Sen's Slope Estimator (Q)

Sen's Slope Estimator (Q) is used to determine the magnitude of trend in a time series. A negative Q imply a decreasing trend and vice-versa. For a given time series(x) of length N, where x_i and x_j are observation or

measured values at i th and j th time scale. The Sen's slope estimator is computed as follows in Equation 4 (Nunes and Lopes, 2016; Sun *et al.*, 2016; Dawood and Atta-ur-Rahman, 2017):

$$Q_i = x_i - x_j / i - j \quad \text{where } i = 1, 2, 3, \dots, N \quad (4)$$

The Q values is computed N time and rearranged in increasing manner. If N is odd, then the median of Q is computed using Equation 5 but when N is even the median Q is computed using Equation 6.

$$Q_{med} = Q[N+1]/2 \quad (5)$$

$$Q_{med} = Q[Q_{N/2} + Q_{N+2/2}]/2 \quad (6)$$

2.3.3. Principal Component Analysis (PCA)

PCA is a multivariate information investigation tool, which lessens or breaks down a multi-dimensional information into a little factor, which still contains the data from the first information. PCA turn the multi-dimensional data into another measurement co-ordinate framework which is orthogonal eigenvectors of the old measurement and contain the greatest difference (Huang *et al.*, 2014a; Dyn *et al.*, 2016). This makes PCA a change centre approach in breaking down information. PCA breaks down a watched between associated variable into new littler straight uncorrelated variable or modes, which clarify the variety in the time arrangement. The modes are masterminded by the level of clarified variety in a sliding request. For a spatio-temporal time series, the spatial examples are portrayed by the eigenvectors, alluded to as experimental orthogonal capacities (EOF) in this study, while the eigenvalues (Principal Component, PC) depict the differences in the time area. The quantity of the clarified parts perfect for deciding the variety ought to be more noteworthy than 70% (Huang *et al.*, 2014a; Dyn *et al.*, 2016; Van Looy *et al.*, 2017). Subtle elements to the usage of PCA can be found in Kolivras and Comrie (2007); Hsu and Li (2010); Navarra and Simoncini (2010); Mberego *et al.* (2013); Huang *et al.* (2014a); Vicente-Serrano *et al.* (2015); Liu and Menzel (2016).

3. RESULTS AND DISCUSSIONS

3.1. Precipitation Variation in UER

The temporal variation of annual precipitations across UER is represented in Figure 2 (blue line). The highest and lowest annual precipitation from 1981 to 2016 were 808 mm yr⁻¹ and 1013 mm yr⁻¹ respectively, which occurred in 1982 and 1996 separately.

The annual precipitation across UER indicated fluctuation variances in between years Figure 2 and a standard deviation of 105.6 mm yr⁻¹. Precipitation in UER between 1981 to 2016 had seen a significant increase of 2.22 mm yr⁻¹ Figure 5 however precipitation decreased during the periods of 1997-2003 and 2010-2014.

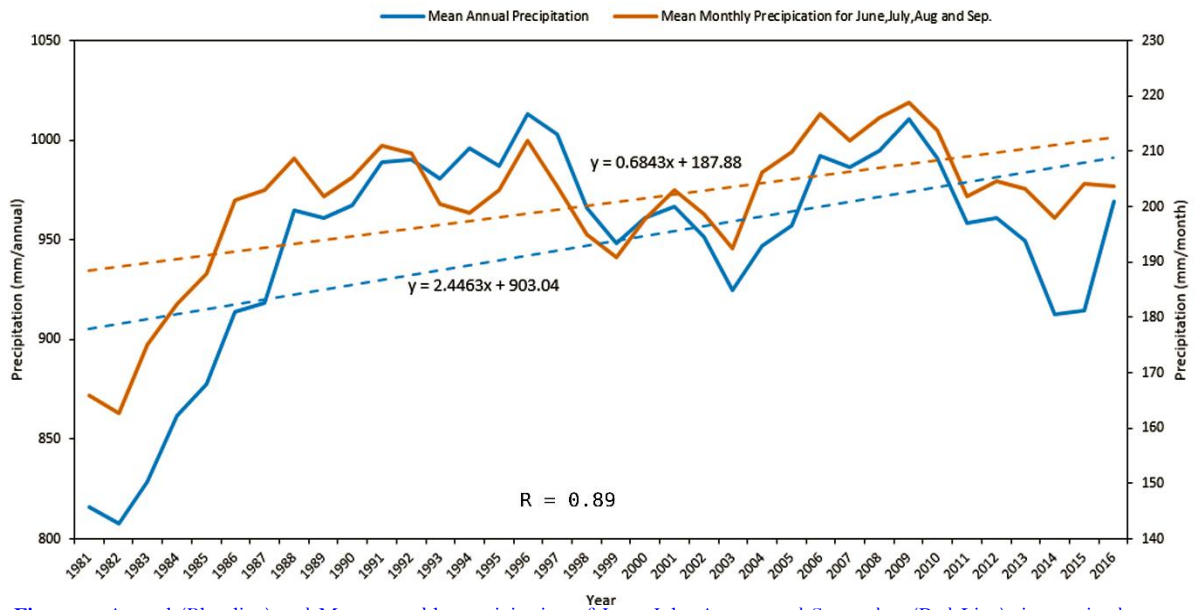


Figure-2. Annual (Blue line) and Mean monthly precipitation of June, July, August and September (Red Line) time series between 1981 and 2016 across UER. The dash lines represent trend line.

The seasonal cycles of precipitation in UER exhibits unimodal pattern Figure 3. In UER, precipitation peak in the month of August with value of 250 mm month⁻¹ which is considerably higher than preceding months. The precipitation month of August accounted for 26.9% of annual precipitation. Standard error was also high in months where high precipitation recorded Table 1. The months of July and September are the second and third most astounding contributors and they accounted for 18.5% and 18.2% respectively to the annual precipitation across UER. The months of July, August and September accounted for 63.6% of the total yearly precipitation. These three months are essential for agriculturists inside UER. The months of January, February and December are positioned twelfth, eleventh and tenth as they contributed 0.1%, 0.2% and 0.2% respectively. All through the study time frame (1981-2016), January, February, March, November and December were noted to be dry with next to zero precipitation. The beginning of the down-pouring season is in April, cresting in August with end starting in October Figure 2. The monthly precipitation contribution of each month is summarized in Table 1.

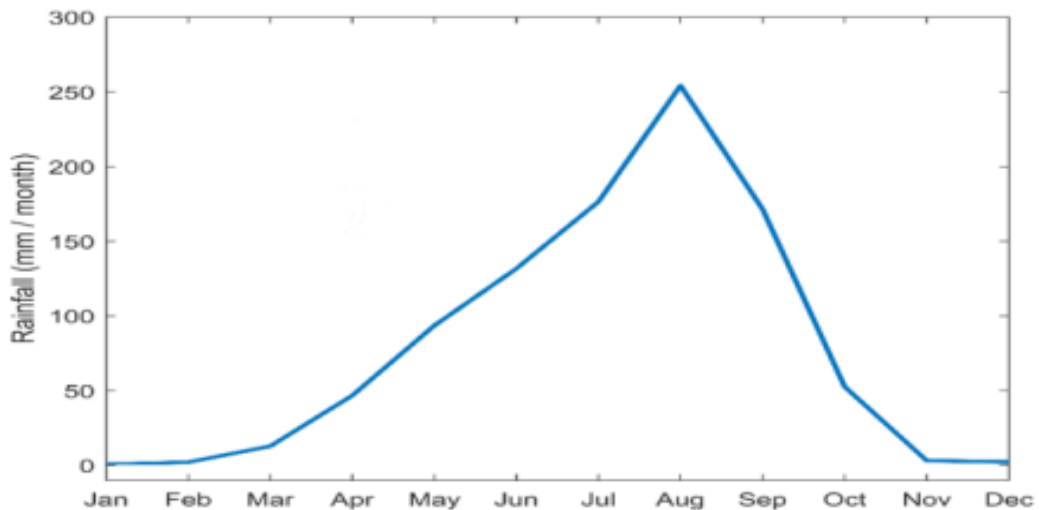


Figure-3. Average monthly rainfall variation between 1981 to 2016 across UER.

The mean annual spatial distribution of precipitation across UER between 1981 to 2016 ranges from 1020mm year⁻¹ to 900 mm year⁻¹ Figure 2. The highest annual precipitation happens around the southern and western part, which the lowest precipitation happens around the north eastern part of UER. The spatially averaged annual

precipitation shows a varying fluctuation throughout the 36 years' study period with coefficient of variation ranging from 11% to 13.5% [Figure 4](#). The highest and lowest coefficient of variation (CV) happens around areas with higher and lower annual precipitation due to annual rate of precipitation ([Liang et al., 2011](#); [Kabo-bah et al., 2016](#)).

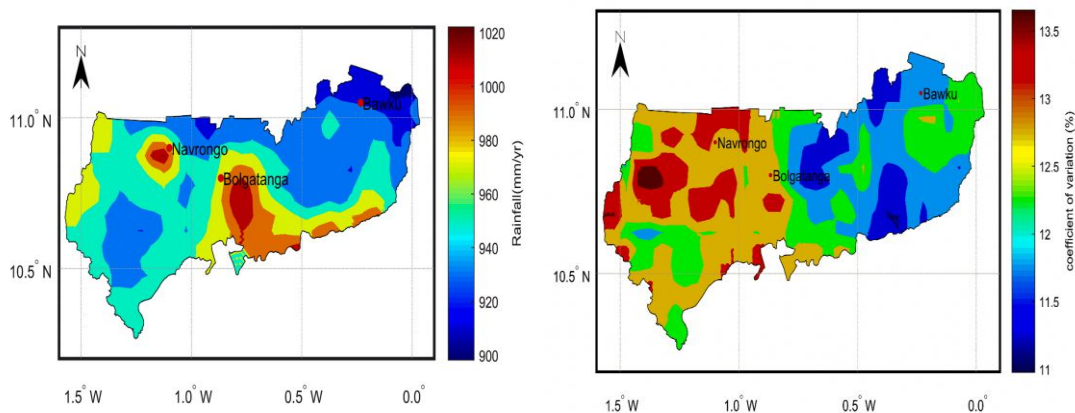


Figure-4. Spatial distribution of mean annual precipitation (a), Coefficient of variation (b) between 1981 and 2016 across UER.

3.1.1. Trend Analysis of Precipitation at Monthly and Seasonal Time Scale

The variation in precipitation across UER were broke down to assessed noteworthy pattern in monthly to determine precipitation design and whether these patterns are increasing or decreasing. The variation in monthly precipitation time series were assessed locally on every pixel at 95% confidence level. The rate of changes in monthly precipitation across UER between 1981 to 2016 fluctuate between $-0.003 \text{ mm month}^{-1}$ and $0.002 \text{ mm month}^{-1}$ [Figure 5\(a\)](#). The decreasing trend was higher in the southern and central part of UER. Within Northeast of UER, the plains of Bawku, the central part (Bolgatanga) and Navrongo located in the north of UER showed decreasing monthly precipitation trend. The highest decreasing trend was measured at the south western ($-0.001 \text{ mm month}^{-1}$ and $-0.002 \text{ mm month}^{-1}$). The highest increasing trend was measured at the eastern part ($-0.001 \text{ mm month}^{-1}$ - $-0.003 \text{ mm month}^{-1}$). The spatial variation of Sen's slope in [Figure 5\(a\)](#) indicated that 55.71% of UER had downward precipitation trend (negative trend) while 44.29% has upward trend. The areas with significant monthly precipitation trends are showed in [Figure 5\(b\)](#).

Precipitation variation in down-pouring months of May, June, July, August and September from 1981 to 2016 were assessed utilizing Mann-Kendall test and Sen's Slope estimator at 95% confidence interval [Figure 8](#). Moreover, the temporal assessment was performed on all 12 months and summarized in [Table 1](#). Precipitation in the month of May, June, November and December showed significant downward trend [Table 1](#). However, the rest of the months showed insignificant upward trend in Precipitation 95% confidence level [Table 1](#). The largest downward trends occurred in May ($-0.43 \text{ mm month}^{-1}$) and June ($-0.35 \text{ mm month}^{-1}$). The largest upward trend was $0.98 \text{ mm month}^{-1}$ and $0.76 \text{ mm month}^{-1}$ that occurred in the months of September and October respectively.

During the 36 years' study period, monthly precipitation in May showed 94.81% of UER had decreasing precipitation trend while 5.19% of the study area had increasing precipitation trends [Figure 7](#). The precipitation in month June showed 97.58% of the region had a negative trend and 2.42% positive trend [Figure 8](#). Majority of UER precipitation in July, August and September demonstrated positive trend [Figure 9-11](#). The percentage area of UER with negative trend in the month of July, August and September are 2.42%, 5.19% and 3.46% separately. The significant maps are showed where black indicates significant trend ($H = 1$) while white indicate insignificant trend ($H = 0$). The areas with higher downward precipitation trends across UER where situated at the north eastern part, central UER and when moving toward the western part of UER. Majority of UER precipitation during September and July had significant trend (Black).

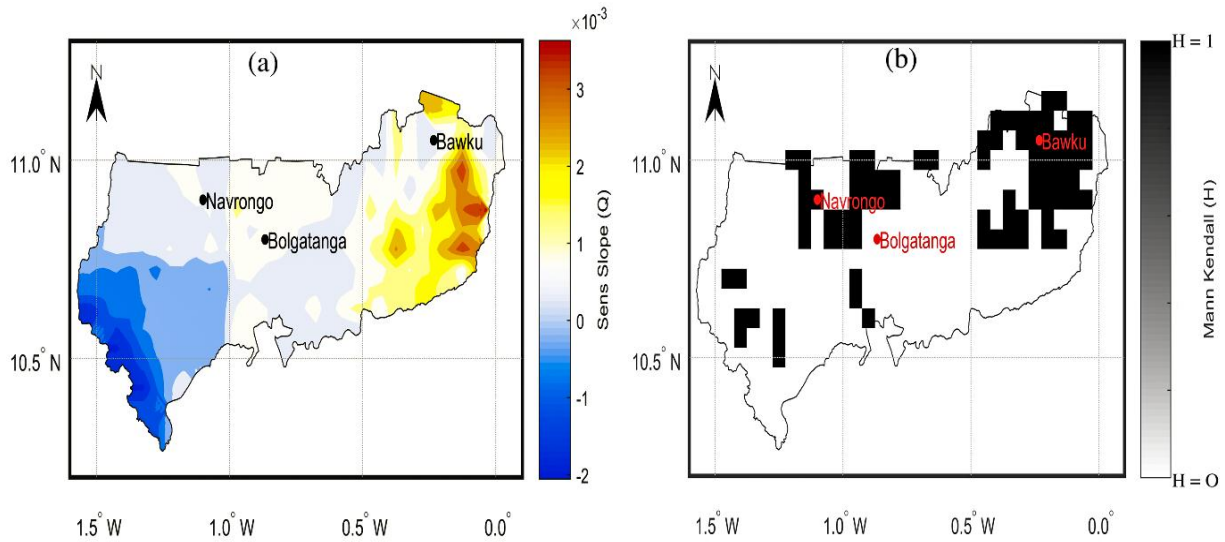


Figure-5. Trend in monthly precipitation between 1981 and 2016 in UER. (a) Spatial variation of Sen's Slope estimator (Q) (b) Mann-Kendall significant trend test showing areas with significant (black) and insignificant (white) trend in precipitation at 95% confidence level.

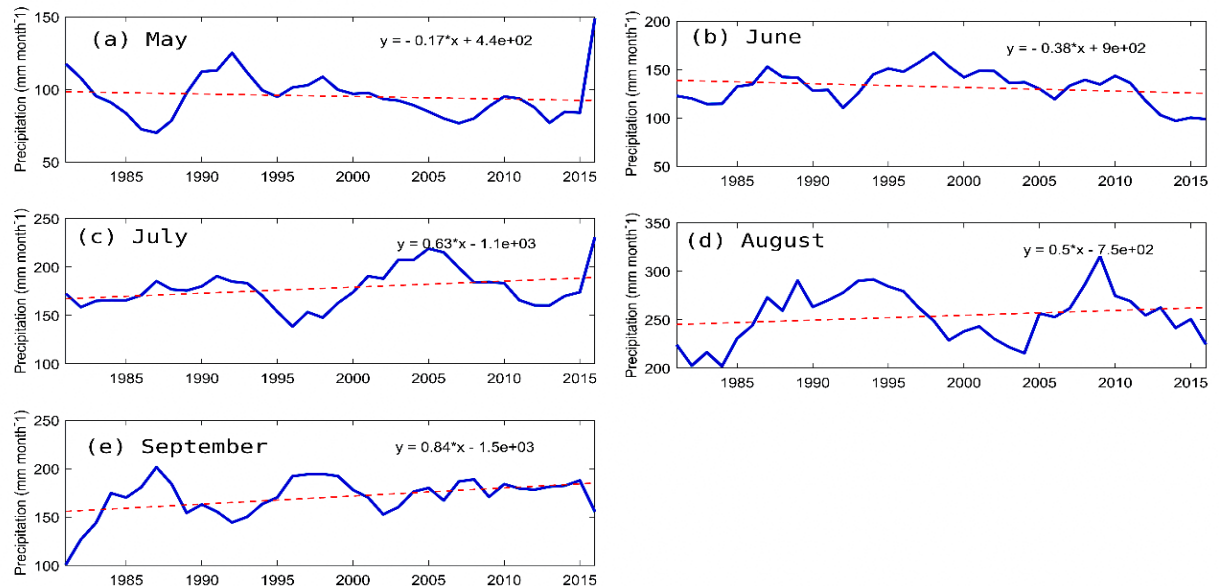


Figure-6. Variation of monthly Precipitation from 1981 to 2016 during (a) May (b) June (c) July (d) August and (e) September. The red dash lines are the trend lines.

Similar to spatial variation of monthly precipitation across UER, precipitation trend in rainy months also varies. May precipitation rate decreased and ranges from -0.2mm month^{-1} to -0.8mm month^{-1} across UER Figure 7. Only few selected areas had significant changes were found in decreasing trends. The range of trends for June precipitation was fluctuate between -1mm month^{-1} to 0.5mm month^{-1} Figure 8. However, majority (almost all) of the surface area of UER had downward trend measured insignificant (white) for May precipitation with the exception of Bolgatanga where significant trend was detected Figure 8(b). The precipitation in July showed an upward trend across UER Figure 9. It is notable that precipitation increased in most areas of UER from the 1981–2016 study period. Both August and September precipitation showed large area increased in upward trend Figure 10,11. The variation in precipitation during June, July, August and September resulted in determining annual precipitation variation across UER Figure 2. These months are primarily attributed to the change in annual precipitation ($R = 0.89$). This results are similar to those that conclude that annual variation in June-July-August (JJA) precipitation reflected the annual variation in precipitation across savanna region of Ghana (Baidu *et al.*, 2017).

The underlying three months (May, June and July) in the major raining period are important to farmers since these are the periods were land preparation and planting takes place (Yiran *et al.*, 2012). Moreover, decreasing trend

in precipitation amid these months implies that planted seeds won't have enough precipitation for germination, and furthermore increment the climatic weight on the sprouted seeds. Research has demonstrated that plant requires water at various phases of development and a solid positive relationship amongst precipitation and vegetation was obtained at various stages, ideal from germination period to the propagation arrange (Ji and Peters, 2003; Lacombe *et al.*, 2012). A decrease in precipitation or water deficiency amid the germination time period will limits cell division and expansion of plant bringing about lessened yield. On the off chance that the agriculturists delayed the planting, the cultivating time period will shorten and along these lines less water would be accessible amid developing phases of the germinating seed. This can be clarified by the sharp lessening in precipitation from the pinnacle precipitation in August to October. The outcomes are similar to those obtained by Yiran *et al.* (2012). These authors reported the complaint from farmers about the adjustments at the beginning of downpours and diminishing length of raining period prompting decreased food crop.

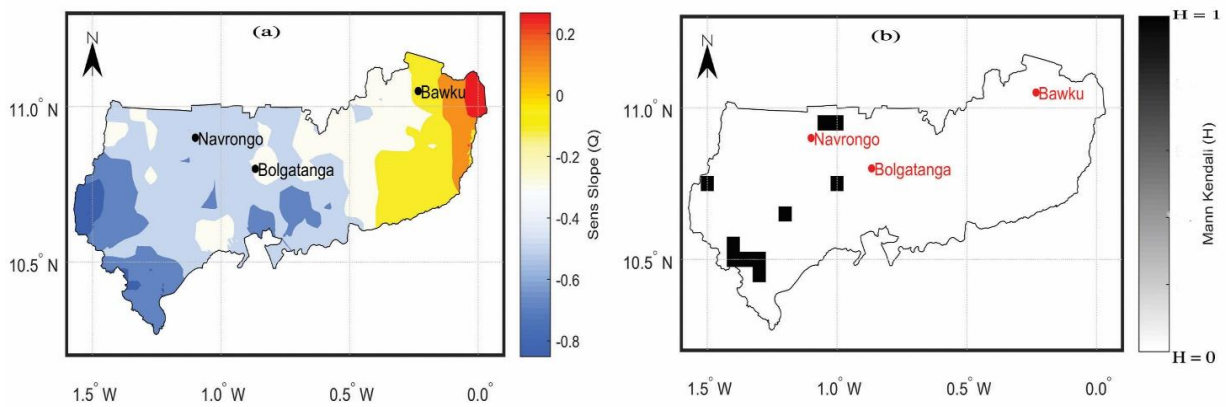


Figure-7. Spatial variation in (a) Sen's Slope estimator (Q) (b) Mann Kendall (H) during the month of May.

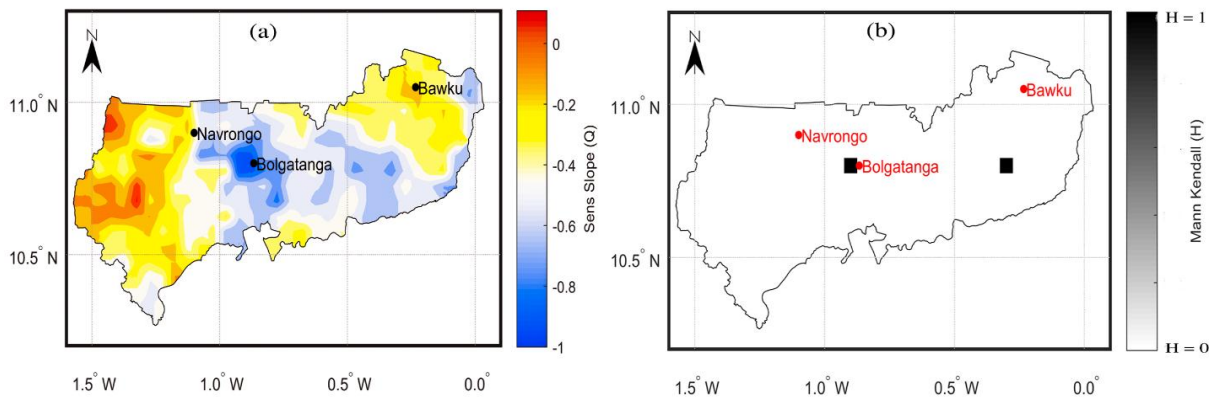


Figure-8. Spatial variation in (a) Sen's Slope estimator (Q) (b) Mann Kendall (H) during the month of June.

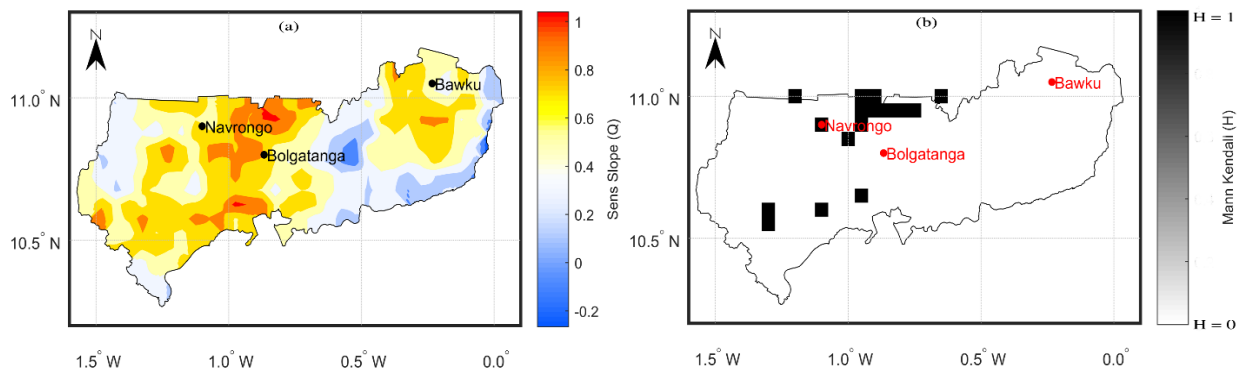


Figure-9. Spatial variation in (a) Sen's Slope estimator (Q) (b) Mann Kendall (H) during the month of July.

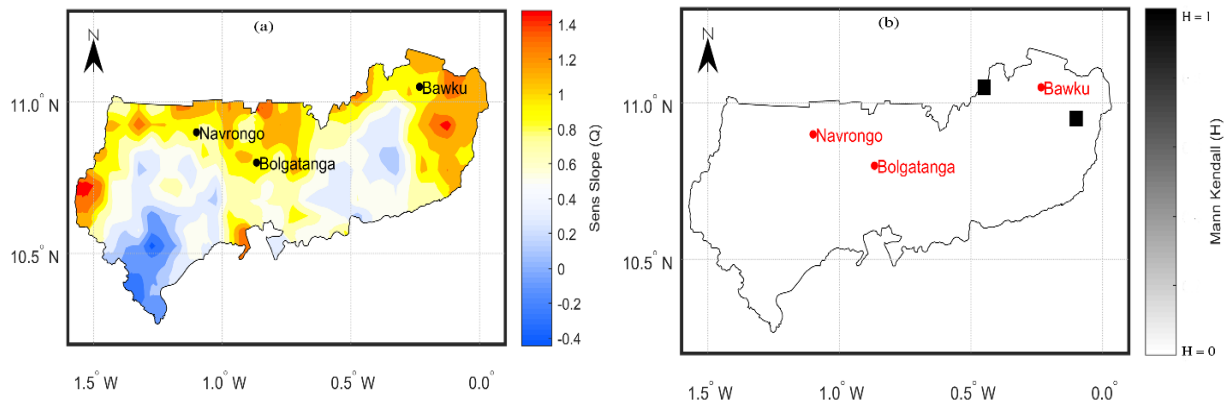


Figure-10. Spatial variation in (a) Sen's Slope estimator (Q) (b) Mann Kendall (H) during the month of August.

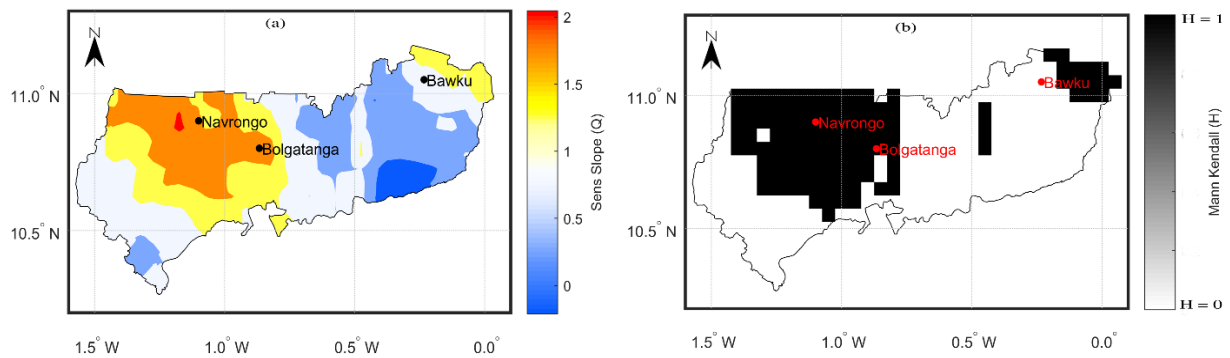


Figure-11. Spatial variation in (a) Sen's Slope estimator (Q) (b) Mann Kendall (H) during the month of September.

Table-1. Mann Kendall (H), Sen's Slope estimator (Q) and contribution of each monthly rainfall in the UER from 1981 to 2016.

Months	Mean(mm)	%Contribution	Ranks	Min(mm)	Max(mm)	Sen's Slope (Q)	Mann Kendall(H)	p-value
Jan.	0.6	0.1	12	0.6	0.7	0.0001	0	0.692
Feb.	2.1	0.2	11	1.5	4.3	0.0013	0	0.902
Mar.	12.5	1.3	8	3.9	28.7	0.0203	0	0.859
Apr.	46.7	4.9	7	14.2	95.8	0.0061	0	0.989
May.	92	9.7	5	51	190.8	-0.4324	1	0.437
Jun.	132.6	14	4	69.8	218.8	-0.3505	1	0.487
Jul.	174.9	18.5	2	101.9	246.5	0.513	0	0.406
Aug.	255	26.9	1	152.4	412	0.6732	0	0.487
Sep.	171.9	18.2	3	100.7	256.6	0.9864	0	0.138
Oct.	53.2	5.6	6	5.1	123.5	0.7594	0	0.037
Nov.	3.2	0.3	9	1.7	11.3	-0.0099	1	0.362
Dec.	2.3	0.2	10	1.9	6.3	-0.0019	1	0.391

Bold row = significant trend (H = 1) at 95% confidence interval.
 Increasing trend = positive (+) and Decreasing trend = negative (-).

3.1.2. Trend Analysis of Precipitation at Annual Time Scale

At the annual time scale, showed an increasing trend in precipitation between 1981 to 2016 Figure 5. Majority of annual precipitation in UER had an upward trend, the diminishing patterns are situated at the northeastern part shifting toward the centre while the entire western piece of the investigation territory had an increasing trend. Some selected areas in the southeastern part also demonstrated increasing pattern in precipitation. The results of the Mann-Kendal test and Sen's slope estimator are displayed in Figure 12 (a-b), where 0.70% of the study area shown significant changes in precipitation while 99.30% shown no significant changes.

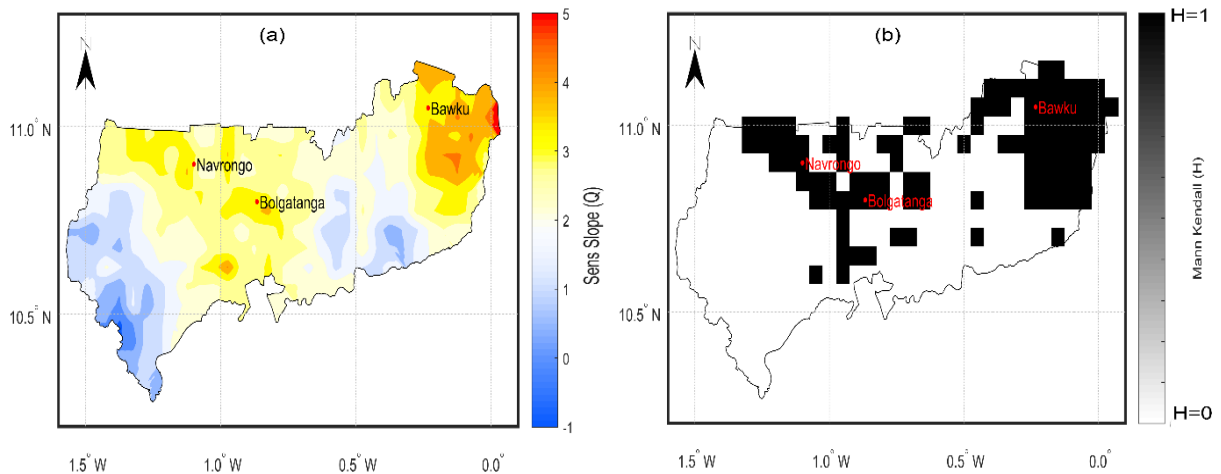


Figure-12. Trend in annual precipitation between 1981 and 2016 in UER. (a) Spatial variation of Sen's Slope estimator (Q) (b) Mann-Kendall significant trend test showing areas with significant (black) and insignificant (white) trend in precipitation at 95% confidence level.

3.2. Change-Point detection in Precipitation Time Series

The Cumulative Residual Analysis (CRA) technique was executed by finding the mean precipitation from 1981 to 2016 and subtracting from annually precipitation to decide the residuals. The annually residuals were then summed in total over the review time frame to recognize changes. There are two notable change points which occurred during 1986 and 2011 **Figure 13**. Based on CRA, the early abrupt change in annual occurred in 1986 due to continuous downward trend in precipitation between 1981-1985. During this period, Ghana experience several droughts which resulted in famine and electrical outages (Bekoe and Logah, 2013). There was an unflinching upward trend in precipitation despite the fact that it is underneath the mean line from 1986 until 2008.

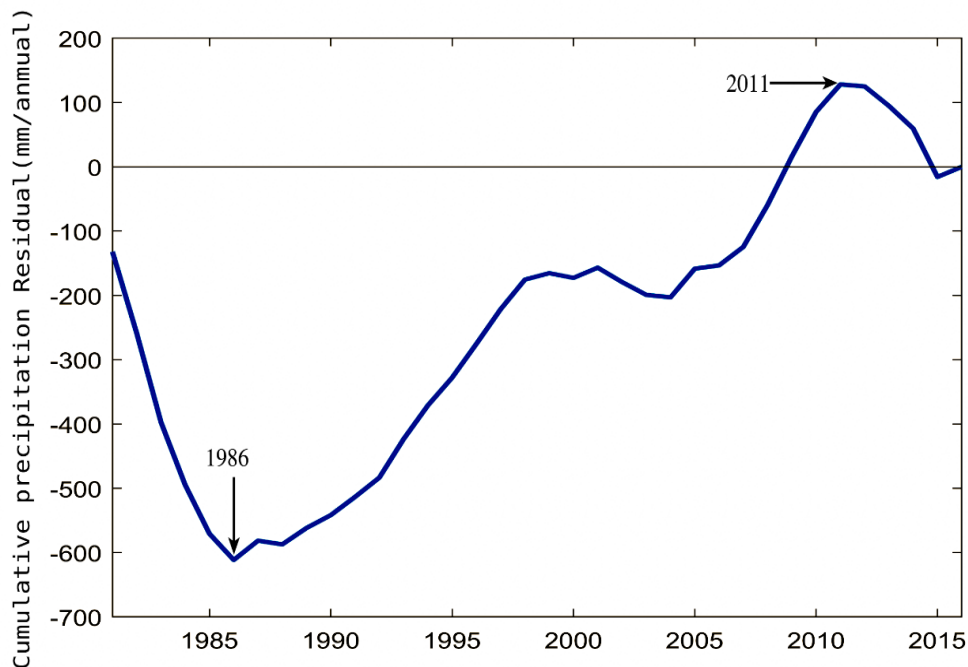


Figure-13. Cumulative annual precipitation residual across UER between 1981 and 2016.

The second major change happened in 2011, where precipitation decreased until 2016. However, these major changes there were additionally various minor changes that happened across UER. The outcomes uncovered that the occasional low peak and high trough demonstrate indications of dry season seriousness in the study area.

3.3. Precipitation Variation Using Wavelet Transform (WT)

The periodicity in precipitation variation was evaluated utilizing WT. This is on account of precipitation information comprises of a grouping of densities that can be adequately dealt with by wavelets transform (Dale and Mah, 1998). Aside from wavelet abilities in analyzing time-frequency domain, it can identify different highlights in the time-series information, for example, the scale, power and normality. The wavelet difference plot can be utilized to assess multi-scale time series. Furthermore, WT application on time series has picked up prevalence because of its capacity to decomposed non-stationary information into a defused time-frequency scale (Santos and Freire, 2012; Sun *et al.*, 2016). The defused time-frequency enables the period of precipitation variation concentration to be detected rather than just the magnitude. Additionally, it enables acquiring detail on both adequacy and how it shifts in time (Torrence and Compo, 1998; Santos and Freire, 2012; Sun *et al.*, 2016). The Morlet mother wavelet was used in the decomposition process.

The WT periodicity results of monthly precipitation are presented in Figure 14. The amplitude of monthly precipitation across UER between 1981 to 2016 is showed in Figure 14(a). The decomposition of monthly precipitation into defused time-frequency space (Wavelet Power Spectrum) is illustrated in Figure 14(b). The Wavelet Power Spectrum (WPS), demonstrate where the periodicity of variation (power) is concentrated which is around 1-year (annual) and 0.5-year period. This is also depicted by Global Wavelet Power Spectrum (GWPS) in Figure 14(c). Figure 15(c) represents the Global Wavelet Power Spectrum (GWPS) which depicts the variance in a period arrangement (Santos and Freire, 2012; Huang *et al.*, 2014a). There are a number of high extreme events in precipitation which occurred in 1990,1995, 2000,2004 and between 2006-2012 Figure 15(b)). However, few of these events occurred at the 6 months' period between 1981 and 2016. During 1986 and the period between 2011 and 2016 the variance in the 0.5-year period band is significantly slight above the 95% confidence level (dash red line) in Figure 14(c). Between 1990 and 2011 all the extreme events at the 1-year period correspond with events at 0.5 year shorter periods. The dark U-shape in Figure 14(b) is the cone of influence where the variance is lessened by padding the time series with zero toward the start and end. This decreases the blunders present when the length of the time arrangement is limited (Santos and Freire, 2012). The variance around the annual cycle (1-year period) is average and resented in Figure 14(d). This demonstrates how the change in the power focus around 1-year cycle period is shifting with time. The differing power fixation indicates how precipitation fluctuates from dry and wet periods above 95% confidence level (dash red line) in UER. Various dry periods with decreasing variance can be identified during 1989-1991, 1994-1998, 1999-2002 and 2013-2015. The energy of the fluctuation likewise demonstrates various wet periods during 1984-1988, 1992-1994, 2003 and 2004. It is important that the generally dry period of 1983, 1990, 2002 and 2013 corresponded with El Nino occasions with lower than normal precipitation. This is similar to the results obtained by Nicholson *et al.* (2000) and Baidu *et al.* (2017).

3.4. Spatial Variation of Precipitation

The spatial variability in precipitation was assessed using Principal Component Analysis (PCA) to decide inconstancy in monthly precipitation between 1981 to 2016 across UER. The results of the spatial variation of precipitation across UER between 1981 to 2016 are showed in Figure 16. The percentage of explained variance of each Principal Component loadings (PC) is showed at the base of each map. The six (6) PC loadings gives an aggregate of 76.52% explained variation, which is above the threshold of 70% (Huang *et al.*, 2014a). The main components were rotated using varimax method to enhance, amplify the connection and creating of areas amongst factors and the segments (Huang *et al.*, 2014a). The varimax rotation technique is a typical orthogonal method of rotating multivariate dataset because of its capacity to lessen complex spatial patterns by separating regions with similar temporal variability (Zhao *et al.*, 2012).

The spatial pattern of loadings delimited the sub-regions that experienced similar precipitation variability in the study period. As shown in Figure 14(a-f), six sub-regions were distinguished (northeast of UER, northeastern

and western of UER, north western of UER, most of middle UER, the middle toward the western area of UER, easternmost of UER). The first principal mode (PC-1) Figure 14a explained the greatest variance of 35.46%, which correspond with area having the least annual precipitation Figure 3(a). This sub-region is situated at the north-eastern (around Bawku) part of the study area. This area additionally indicates huge downward trend in monthly precipitation Figure 6(a-b). The second principal mode (PC-2) Figure 14b explained 17.46% of the variation and had its anomalies located at western and northeastern part of the study area. This sub-region corresponds to places with low to medium mean annual precipitation ranging from 640 mm annual⁻¹ to 980 mm annual⁻¹ Figure 3(a). The third principal mode (PC-3) Figure 14c explained 11.15% of precipitation variation across UER. The highest anomaly is distributed around the north-western part and this correspond to location with high mean annual precipitation (940 mm annual⁻¹ – 1020 mm annual⁻¹). The fourth principal mode (PC-4) and fifth principal mode (PC-5) have their highest anomalies around the middle and toward the western part of UER and they explained 5.23% and 4.06% of precipitation variation. The most important pattern in this sub-regions are central/northwest mode of anomalies. The highest anomalies in the sixth principal mode (PC-6) are distributed around Bawku in the northeastern, and the lowest anomalies are in the north of UER. A similar northeastern precipitation anomaly could be found in the first principal mode (PC 1). This sub-region (zone) is unique due to its active land degradation (Yiran *et al.*, 2012) and decreasing tend in monthly precipitation (Baidu *et al.*, 2017).

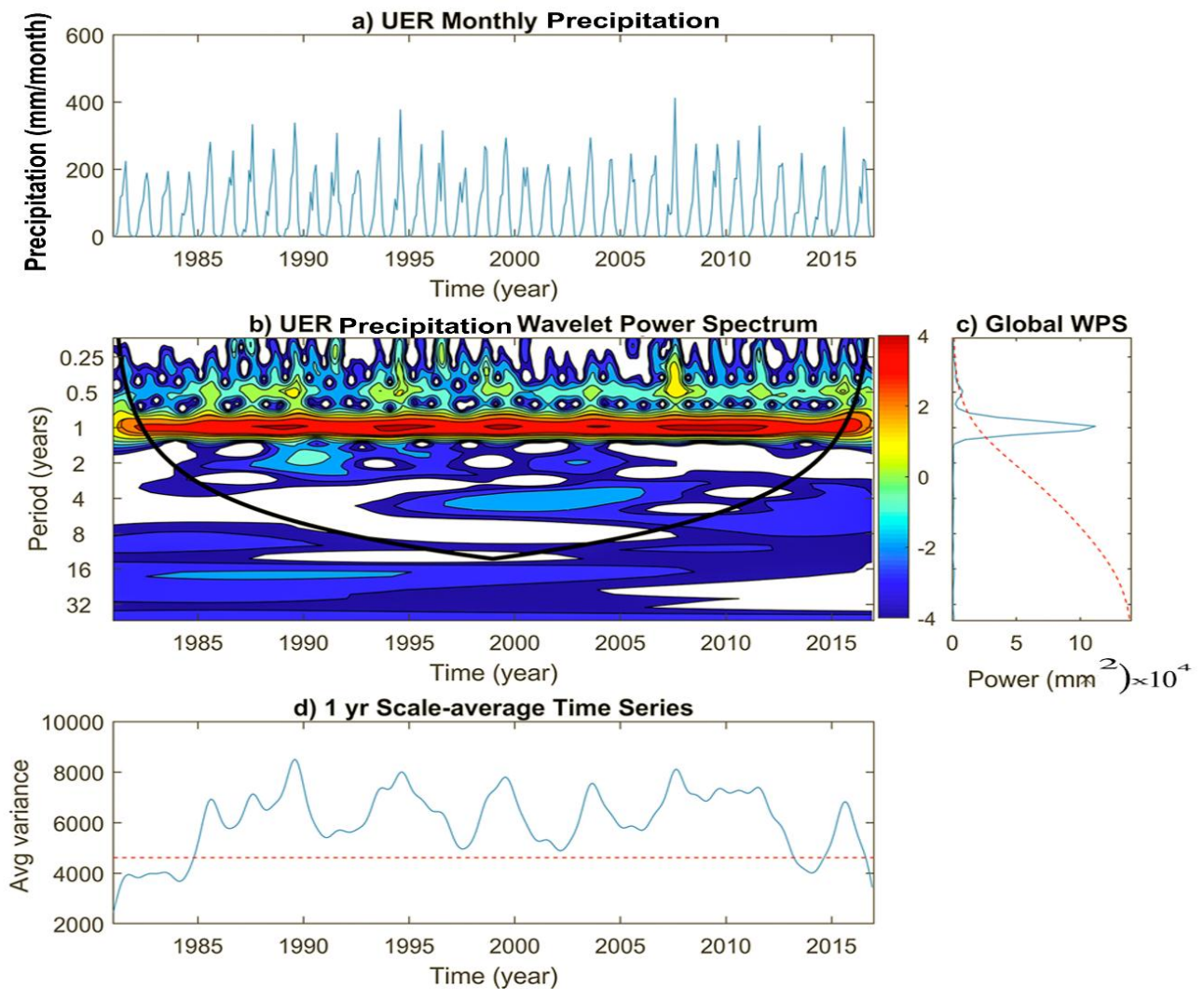


Figure-14. (a) Monthly rainfall pattern in UER from 1981-2016; (b) Wavelet Power Spectrum (WPS) which indicates the variance of the power concentration in the time series; (c) Global Wavelet Power Spectrum (GWPS); and (d) Scale average of power around 1-year period.

Additionally, to further understand the temporal variation of precipitation across these sub-regions, the corresponding principal components scores for each PC loading were investigated in Figure 16. The eigenvalues of each PC's known as PC score measures the contribution of monthly precipitation variance to the total variance in precipitation time series and could likewise be interpreted as the temporal modulation of every PC's Figure 16(a-f). PC-1, PC-3 and PC-4 scores were positively correlated ($R_1 = 0.27$, $R_3 = 0.70$, $R_4 = 0.03$) with 3 months moving average of monthly precipitation over the study period. Furthermore, PC-5 and PC-6 were positively correlated ($R_5 = 0.06$, $R_6 = 0.36$) with 7 months and 5 months moving average respectively. However, PC-2 had no correlation with 3,7 and 1 year moving of monthly precipitation. Additionally, PC-1, PC-3, PC-4, PC-5 and PC-6 all demonstrated a positive correction with 3 and 5 months moving average of monthly precipitation.

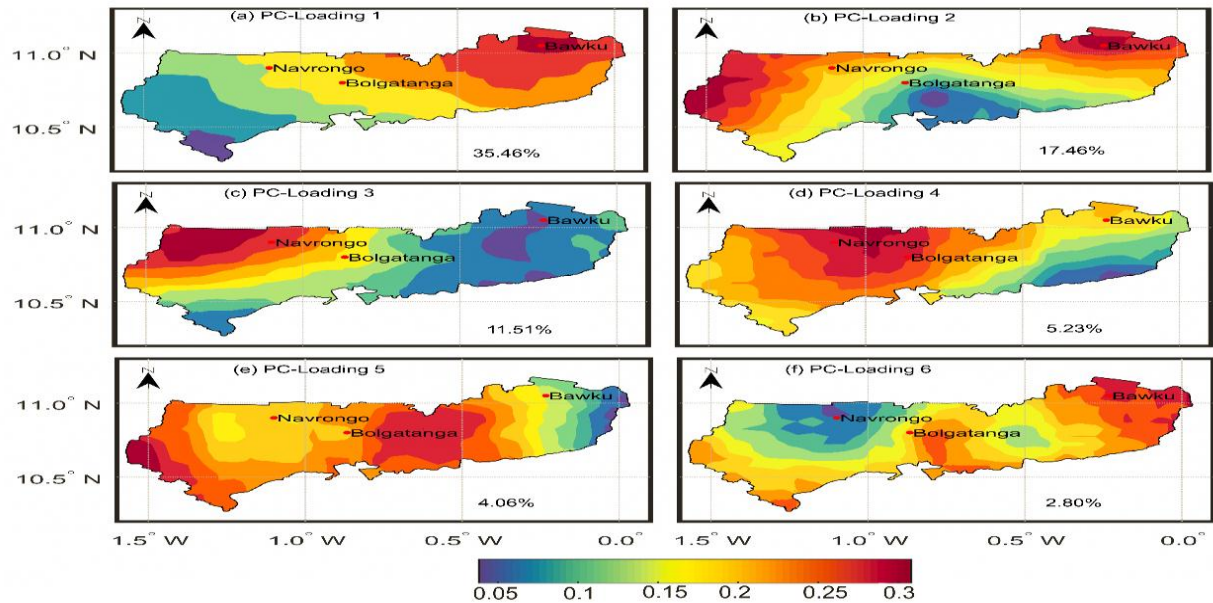


Figure-15. Spatial pattern of first five rotated PC modes ('Loading') of precipitation variation across UER between 1981 to 2016. The percentage of explained variations is represented below in percentage.

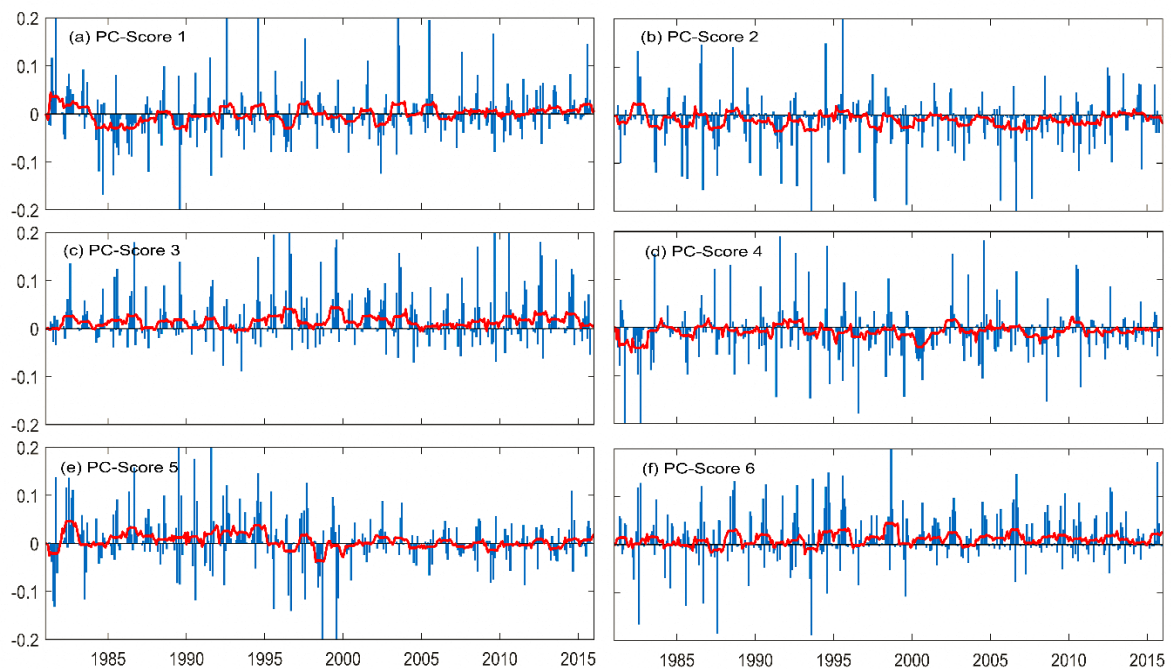


Figure-16. Time series of the first five Principle Components (PC) scores modulation. The red line 13 months moving average.

These findings demonstrate that PC-1, PC-3, PC-4, PC-5 and PC-6 represent intra-annual variation in monthly precipitation. It could be noted from the 12 months moving average plot red line in Figure 17 that years in which every one of the plots demonstrates valleys (diminished in size) relate to a period with downward trend in precipitation. This outcome harmonizes with the outcomes from CRA and WT for the years 1983, 1984, 1985, 1990 and 2000.

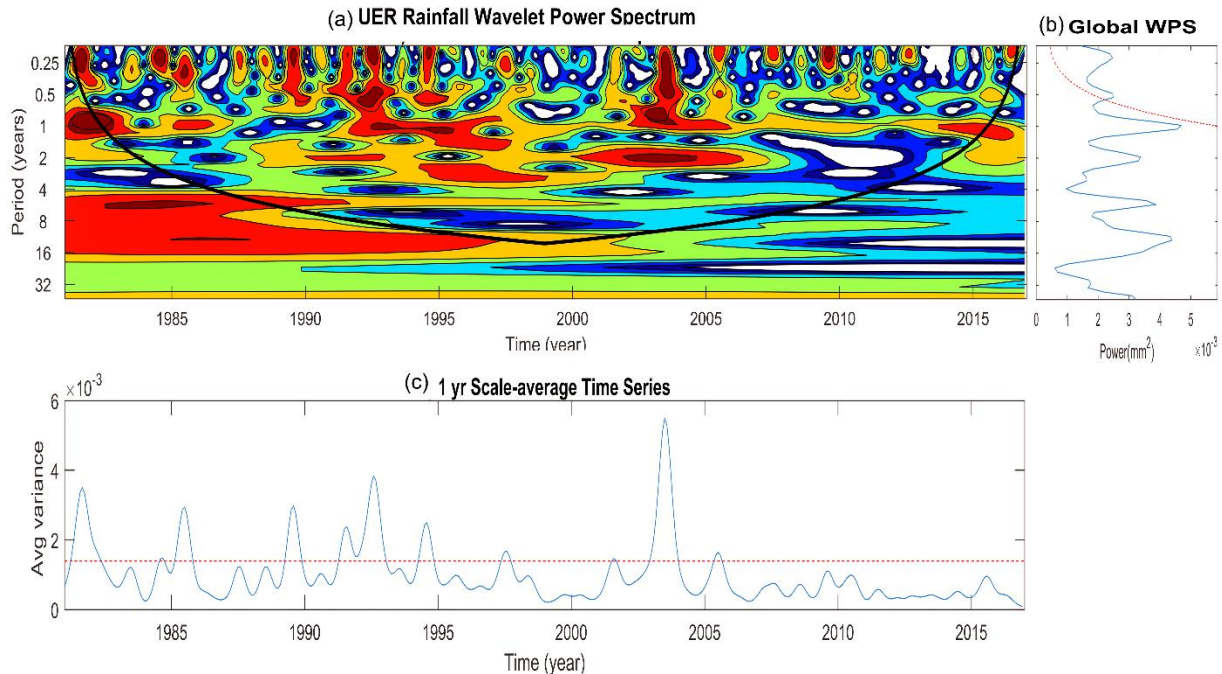


Figure-17. (a) Wavelet power spectrum (WPS) which indicates the variance of the power concentration in the time series of PC Score 1 (b) Global Wavelet Power Spectrum (GWPS) and (c) Scale average of power around 1-year period.

Finally, PC-1 is the main precipitation variation across UER, further analysis using wavelet transform technique was applied to detect the periodicity of dryness/wetness. A 3 months to 4-year periodicity characteristic could be noticed over the sub region Figure 15(a). A number of high extreme events in precipitation occurred at totally different period between 1981 to 2016 (Red contour in Figure 17(b)). However, few of these events occurred at 3-months to 2 years' period. The variance around the around 1-year period is average and resented in Figure 17(c). Various extreme events occurred periods with decreasing variance can be identified during 1989-1991, 1994-1998, 1999-2002 and 2013-2015. The energy of the fluctuation likewise demonstrates various wet periods during 1984-1988, 1992-1994, 2003 and 2004.

4. CONCLUSIONS AND RECOMMENDATIONS

Over the 36 years study period, August contributed 26.9% of the aggregated yearly precipitation in the study area. This is trailed by July (18.5%) and September (18.3%). The last contributors are January (0.1%), February (0.2%) and December (0.2%). The precipitation in the study region takes after a unimodal precipitation design which begins from April/May and crests in August before consummation in October. Evaluating the trends in precipitation time series utilizing Mann-Kendall and Sen's slope estimator uncovered that exclusively 27.34% of the aggregate surface area demonstrated a significant trend in precipitation, while 44.29% of UER region demonstrated an increased in precipitation amid the 36 years contemplate period. From 1981 to 2012, around 90% of the study region's precipitation in May and June experienced a decreasing trend in precipitation. The long stretches of July, August and September demonstrates fluctuating spatial patterns in precipitation time series. For the most part, precipitation across the study area is beneath normal from 1981 to around 2009 and 2010 where it goes over the mean mark. Be that as it may, between these significant years there were events of wet and dry years. From 2013 to

2016, the study area indicates a ceaseless decrease in precipitation. The Wavelet Transforms investigation demonstrates that the variety in precipitation was every year noteworthy. This likewise compares with wet and dry periods. The wet and dry period relates to the aggregate lingering study discoveries in where 1981-1984, 1989-1991, 1994-1998, 1999-2002 and 2013-2015 were noted as dry years. The year 1988, 1992-1994, 2003 and 2004 were recognized as wet periods over UER. These variations in the precipitation fluctuation give a sign the study area is a dry spell inclined region. The spatial variety of precipitation uncovered that the spatial pattern of precipitation is extremely different and can be partitioned into five sub-districts, however, lion's share of the changeability is amassed at the north-eastern segment. Advance investigation demonstrates that the primary (PC-1), second (PC-2) and third (PC-3) sub-regions are decidedly related with 3-months and 5-months moving average of precipitation. The fourth (PC-4) and fifth (PC-5) sub-areas demonstrated positive connection with 13-months moving normal. The outcomes from precipitation 3 months, 5-months and 13 months moving average show precipitation change oddities which are fundamentally decreasing over the UER. This would have a negative impact on horticultural practice with is the fundamental employment in UER, water asset administration and nourishment security.

In addition, the long time span of precipitation data used in assessing the spatial and temporal variety could give a road to dry season appraisal (drought) and the long-term forecast precipitation in UER. The result from this investigation gives a benchmark to powerful and proficient administration, arranging and maintainable advancement for dry season alleviation to enhance horticulture, animals, and so forth in the UER for the present age and secure it for the future age. Also, the results from CHIRPS remotely sensed precipitation data indicated the capacity of the data in assessing spatial and temporal dynamics at regional level.

Funding: This study received no specific financial support.

Competing Interests: The authors declare that they have no competing interests.

Acknowledgement: All authors contributed equally to the conception and design of the study.

REFERENCES

- Andam-Akorful, S., V. Ferreira, C. Ndehedehe and J. Quaye-Ballard, 2017. An investigation into the freshwater variability in West Africa during 1979-2010. *International Journal of Climatology*, 37: 333-349. Available at: <https://doi.org/10.1002/joc.5006>.
- Antwi-Agyei, P., E.D. Fraser, A.J. Dougill, L.C. Stringer and E. Simelton, 2012. Mapping the vulnerability of crop production to drought in Ghana using rainfall, yield and socioeconomic data. *Applied Geography*, 32(2): 324-334. Available at: <https://doi.org/10.1016/j.apgeog.2011.06.010>.
- Awotwi, A., G.K. Anornu, J. Quaye-Ballard, T. Annor and E.K. Forkuo, 2017. Analysis of climate and anthropogenic impacts on runoff in the Lower Pra River Basin of Ghana. *Heliyon*, 3(12): e00477. Available at: <https://doi.org/10.1016/j.heliyon.2017.e00477>.
- Baidu, M., L.K. Amekudzi, J.N.A. Aryee and T. Annor, 2017. Assessment of long-term Spatio-temporal rainfall variability over Ghana Using Wavelet Analysis. *Climate*, 5(30): 1-24.
- Basalirwa, C., J. Odiyo, R. Mngodo and E. Mpeti, 1999. The climatological regions of Tanzania based on the rainfall characteristics. *International Journal of Climatology*, 19(1): 69-80. Available at: [https://doi.org/10.1002/\(sici\)1097-0088\(199901\)19:1<69::aid-joc343>3.3.co;2-d](https://doi.org/10.1002/(sici)1097-0088(199901)19:1<69::aid-joc343>3.3.co;2-d).
- Bekoe, E.O. and F.Y. Logah, 2013. The impact of droughts and climate change on electricity generation in Ghana. *Environmental Sciences*, 1(1): 13-24.
- Blain, G.C., 2013. The modified Mann-Kendall test: On the performance of three variance correction approaches. *Bragantia*, 72(4): 416-425. Available at: <https://doi.org/10.1590/brag.2013.045>.
- Dale, M. and M. Mah, 1998. The use of wavelets for spatial pattern analysis in ecology. *Journal of Vegetation Science*, 9(6): 805-814. Available at: <https://doi.org/10.2307/3237046>.

- Dawood, M. and Atta-ur-Rahman, 2017. Spatio-statistical analysis of temperature fluctuation using Mann–Kendall and Sen’s slope approach. *Climate dynamics*, 48(3–4): 783–797.
- Dyn, C., J. Zhang, Y. Hao, B.X. Hu, X. Huo and P. Hao, 2016. The effects of monsoons and climate teleconnections on the Niangziguan Karst Spring discharge in North China. *Climate Dynamics*, 48(1–2): 53–70.
- Ghana Statistical Service, 2010. Population & housing census. Regional Analytical Report - Upper East Region: Accra.
- Hsu, K.-C. and S.-T. Li, 2010. Clustering spatial–temporal precipitation data using wavelet transform and self-organizing map neural network. *Advances in Water Resources*, 33(2): 190–200.
- Huang, J., Y. Xue, S. Sun and J. Zhang, 2014a. Spatial and temporal variability of drought during 1960–2012 in inner. *Quaternary International*, 10: 1–11. Available at: [10.1016/j.quaint.2014.10.036](https://doi.org/10.1016/j.quaint.2014.10.036).
- IPCC, 2007. 976. *Climate Change 2007: Impacts, adaptation and vulnerability. Contribution of Working Group II to the Fourth Assessment Report of the Intergovernmental Panel on Climate Change*, M.L. Parry, O.F. Canziani, J.P. Palutikof, P.J. Van der Linden and C.E. Hanson, Eds., Cambridge University Press, Cambridge, UK, pp: 976.
- Jarawura, F.X., 2013. Drought and migration In Northern Ghana. PhD. Thesis, Centre for Migration Studies, University of Ghana. Accra, Ghana, 1–223.
- Ji, L. and A.J. Peters, 2003. Assessing vegetation response to drought in the Northern Great Plains using vegetation and drought indices. *Remote Sensing of Environment*, 87(1): 85–98. Available at: [https://doi.org/10.1016/S0034-4257\(03\)00174-3](https://doi.org/10.1016/S0034-4257(03)00174-3).
- Kabo-bah, A.T., C.J. Diji, K. Nokoe, Y. Mulugetta, D. Obeng-ofori and K. Akpoti, 2016. Multiyear rainfall and temperature trends in the volta river Basin and their potential impact on Hydropower Generation in Ghana. *Climate*, 4(49): 1–17.
- Kolivas, K.N. and A.C. Comrie, 2007. Regionalization and variability of precipitation in Hawaii. *Physical Geography*, 28(1): 76–96. Available at: <https://doi.org/10.2747/0272-3646.28.1.76>.
- Lacombe, G., M. McCartney and G. Forkuor, 2012. Drying climate in Ghana over the period 1960–2005: Evidence from the resampling-based Mann-Kendall test at local and regional levels. *Hydrological Sciences Journal*, 57(8): 1594–1609. Available at: <https://doi.org/10.1080/02626667.2012.728291>.
- Le, A.M. and N.G. Pricope, 2017. Increasing the accuracy of runoff and streamflow simulation in the Nzoia Basin , Western Kenya, Through the Incorporation of Satellite-Derived CHIRPS Data. *Water*, 9(114).
- Leemhuis, C., G. Jung, R. Kasei and J. Liebe, 2009. The volta basin water allocation system: Assessing the impact of small-scale reservoir development on the water resources of the Volta Basin, West Africa. *Advances in Geosciences*, 21: 57–62. Available at: <https://doi.org/10.5194/adgeo-21-57-2009>.
- Liang, L., L. Li and Q. Liu, 2011. Precipitation variability in Northeast China from 1961 to 2008. *Journal of Hydrology*, 404(1–2): 67–76. Available at: <https://doi.org/10.1016/j.jhydrol.2011.04.020>.
- Liu, Z. and L. Menzel, 2016. Identifying long-term variations in vegetation and climatic variables and their scale-dependent relationships: A case study in Southwest Germany. *Global and Planetary Change*, 147: 54–66. Available at: <https://doi.org/10.1016/j.gloplacha.2016.10.019>.
- Mberego, S., K. Sanga-Ngoie and S. Kobayashi, 2013. Vegetation dynamics of Zimbabwe investigated using NOAA-AVHRR NDVI from 1982 to 2006: A principal component analysis. *International Journal of Remote Sensing*, 34(19): 6764–6779. Available at: <https://doi.org/10.1080/01431161.2013.806833>.
- Ministry of Food & Agriculture, 2017. Upper East region, Ministry of Food & Agriculture, Ghana. Available from http://mofa.gov.gh/site/?page_id=654 [Accessed 21 February 2017].
- Nalley, D., J. Adamowski, B. Khalil and B. Ozga-Zielinski, 2013. Trend detection in surface air temperature in Ontario and Quebec, Canada during 1967–2006 using the discrete wavelet transform. *Atmospheric Research*, 132: 375–398. Available at: <https://doi.org/10.1016/j.atmosres.2013.06.011>.
- Navarra, A. and V. Simoncini, 2010. *A guide to empirical orthogonal function for climate data analysis*. New York: Springer Berlin Heidelberg.

- Nicholson, S.E., B. Some and B. Kone, 2000. An analysis of recent rainfall conditions in West Africa, including the rainy seasons of the 1997 El Niño and the 1998 La Niña years. *Journal of Climate*, 13(14): 2628–2640.
- Nick, v.d.G., M. Andreini, A.V.A.N. Edig and P. Vlek, 2001. Competition for water resources of the Volta basin, Regional Management of Water Resources (Proceedings of a Symposium Held During the Sixth IAHS Scientific Assembly at Maastricht, The Netherlands, July 2001). IAHS Publication. no. 268, 20011964 (268), 199–205.
- Nischitha, V., S. Ahmed, H. Varikoden and J. Revadekar, 2014. The impact of seasonal rainfall variability on NDVI in the Tunga and Bhadra river basins, Karnataka, India. *International Journal of Remote Sensing*, 35(23): 8025–8043. Available at: <https://doi.org/10.1080/01431161.2014.979301>.
- Nunes, A.N. and P. Lopes, 2016. Streamflow response to climate variability and land- cover changes in the River Beça Watershed, Northern Portugal. *River Basin Management*: 61–80. Available at: [10.5772/63079](https://doi.org/10.5772/63079).
- Paredes-Trejo, F.J., H. Barbosa and T.L. Kumar, 2017. Validating CHIRPS-based satellite precipitation estimates in Northeast Brazil. *Journal of Arid Environments*, 139: 26–40. Available at: <https://doi.org/10.1016/j.jaridenv.2016.12.009>.
- Quagraine, K.A., N. Ama, B. Klutse, F. Nkrumah, D.C. Adukpoo and K. Owusu, 2017. Changes in Rainfall characteristics in Wenchi and Saltpond farming areas of Ghana. *International Journal of Geosciences*, 8(3): 305–317. Available at: <https://doi.org/10.4236/ijg.2017.83015>.
- Retalis, A., F. Tymvios, D. Katsanos and S. Michaelides, 2017. Downscaling CHIRPS precipitation data: An artificial neural network modelling approach. *International Journal of Remote Sensing*, 38(13): 3943–3959. Available at: <https://doi.org/10.1080/01431161.2017.1312031>.
- Santos, C.A.G. and P.K.M.M. Freire, 2012. Analysis of precipitation time series of Urban Centers of Northeastern Brazil using Wavelet Transform. *International Journal of Environmental, Chemical, Ecological, Geological and Geophysical Engineering*, 6(7): 405–410.
- Sun, T., V. Ferreira, X. He and S. Andam-Akorful, 2016. Water availability of Sao Francisco river basin based on a space-borne geodetic sensor. *Water*, 8(5): 1–20. Available at: <https://doi.org/10.3390/w8050213>.
- Torrence, C. and G.P. Compo, 1998. A practical guide to wavelet analysis. *Bulletin of the American Meteorological Society*, 79(1): 61–78.
- Van Looy, K., J. Piffady and M. Floury, 2017. At what scale and extent environmental gradients and climatic changes influence stream invertebrate communities? *Science of the Total Environment*, 580: 34–42.
- Vicente-Serrano, S.M., O. Chura, J.I. López-Moreno, C. Azorin-Molina, A. Sanchez-Lorenzo, E. Aguilar, E. Moran-Tejeda, F. Trujillo, R. Martínez and J. Nieto, 2015. Spatio-temporal variability of droughts in Bolivia: 1955–2012. *International Journal of Climatology*, 35(10): 3024–3040. Available at: <https://doi.org/10.1002/joc.4190>.
- Wang, S., C. Huang, L. Zhang, Y. Lin, Y. Cen and T. Wu, 2016. Monitoring and assessing the 2012 drought in the great plains: Analyzing satellite-retrieved solar-induced chlorophyll fluorescence. *Drought Indices , and Gross Primary Production. Remote Sensing*, 8(61): 1–17.
- Yiran, G., J. Kusimi and S. Kufogbe, 2012. A synthesis of remote sensing and local knowledge approaches in land degradation assessment in the Bawku East District, Ghana. *International Journal of Applied Earth Observation and Geoinformation*, 14(1): 204–213. Available at: <https://doi.org/10.1016/j.jag.2011.09.016>.
- Zhao, G., X. Mu, G. Hörmann, N. Fohrer, M. Xiong, B. Su and X. Li, 2012. Spatial patterns and temporal variability of dryness/wetness in the Yangtze River Basin, China. *Quaternary International*, 282: 5–13.

Views and opinions expressed in this article are the views and opinions of the author(s), International Journal of Geography and Geology shall not be responsible or answerable for any loss, damage or liability etc. caused in relation to/arising out of the use of the content.